Supporting information

Metal-organic framework derived electrical insulating-conductive double-layer structure for stable lithium metal anode

Jianzong Man[a], Wenlong Liu[a], Haibang Zhang[a], Kun Liu[a], Yongfu Cui[b], Jinpeng Yin[a], Xinyu Wang [*a], and Juncai Sun [*a]

[a] Institute of Materials and Technology, Dalian Maritime University, Dalian, 116026, China

[b] School of Transportation Engineering, Guizhou Institute of Technology, Guiyang, 550003, China

[*]Corresponding author: sunjc@dlmu.edu.cn (J. Sun),

wangxinyu@dlmu.edu.cn (X. W)

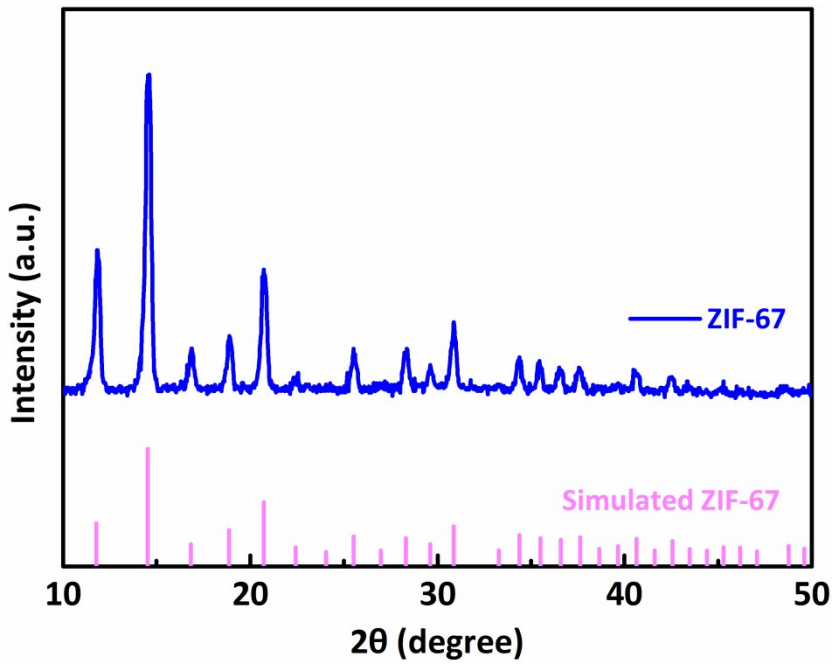

Fig. S1 XRD patterns of ZIF-67 and simulated ZIF-67.

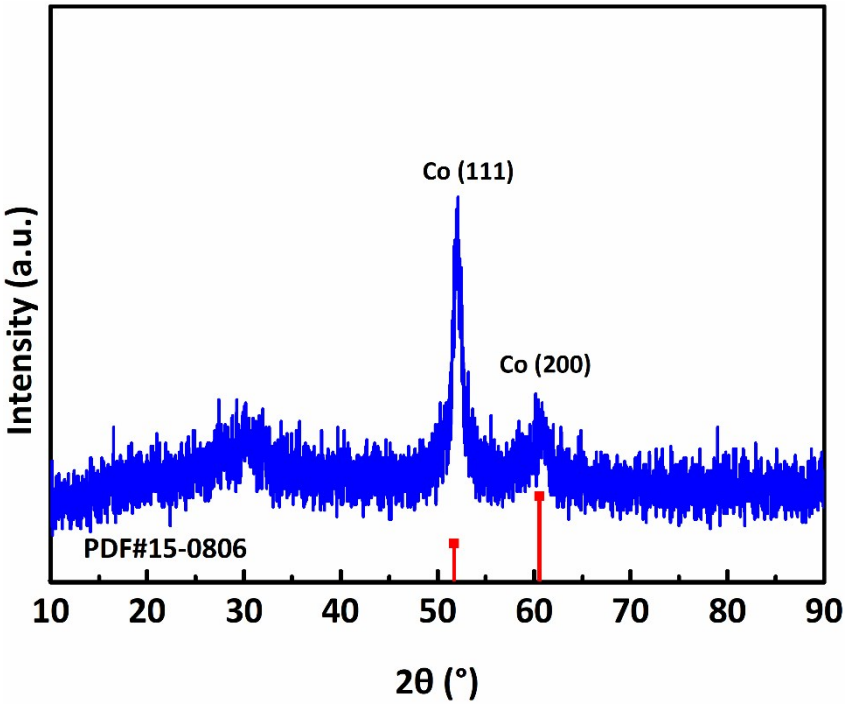

Fig. S2 XRD pattern of Co@NPC.

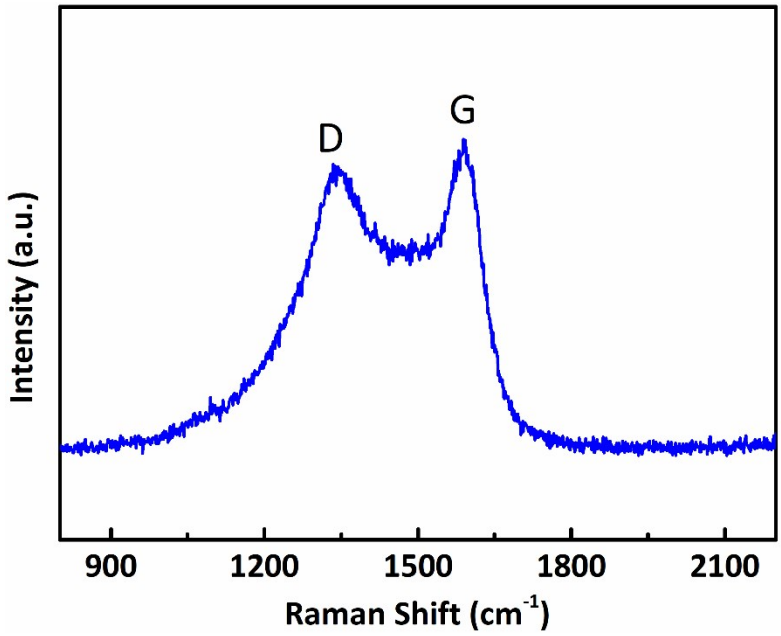

Fig. S3 Raman spectrum of Co@NPC

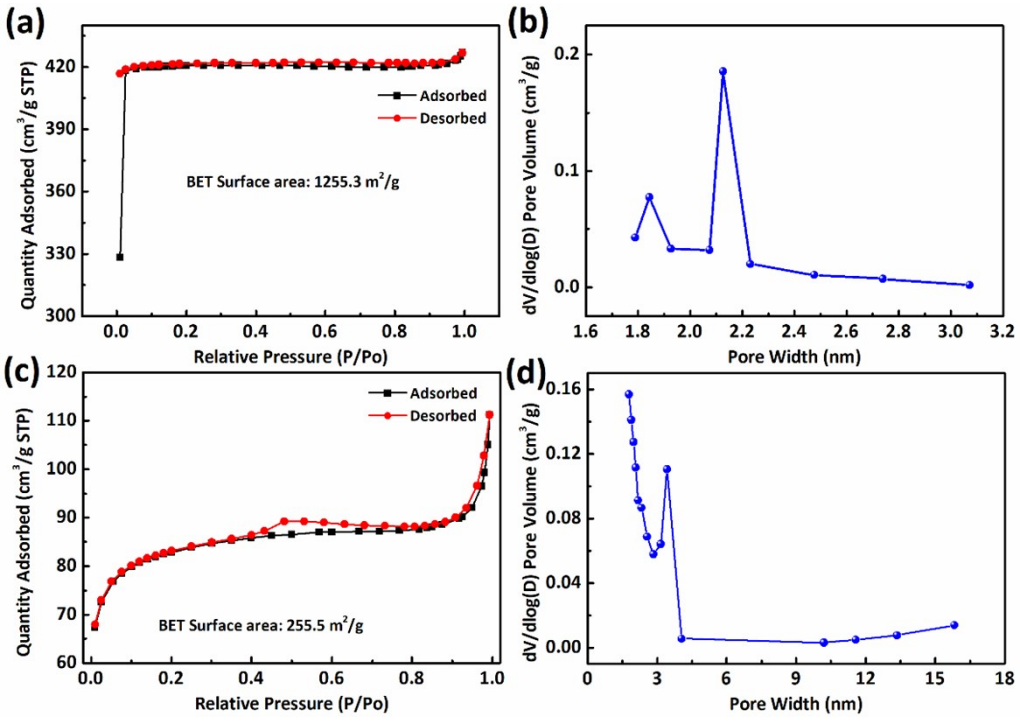

Fig. S4 N_2 adsorption-desorption isotherms of (a) ZIF-67 and (c) Co@NPC, pore size distribution of (b) ZIF-67 and (d) Co@NPC.

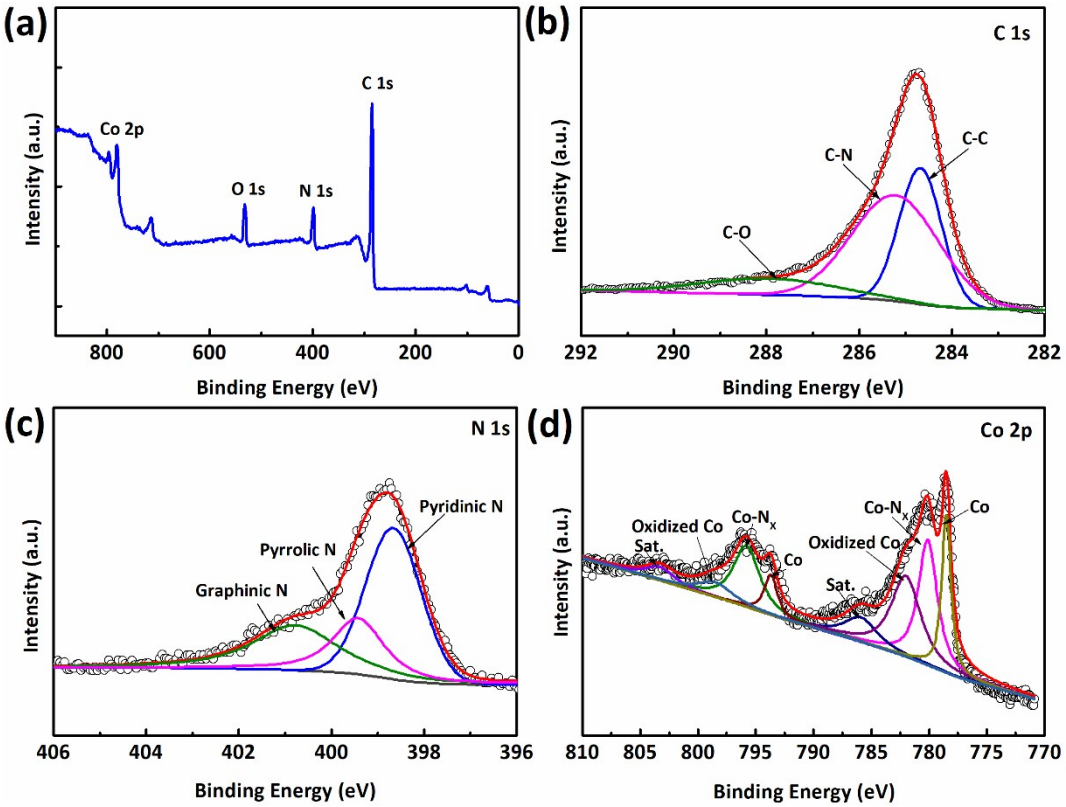

Fig. S5 (a) The XPS survey spectrum of Co@NPC. (b-d) high-resolution of XPS spectrums of C 1s, N 1s and Co 2p.

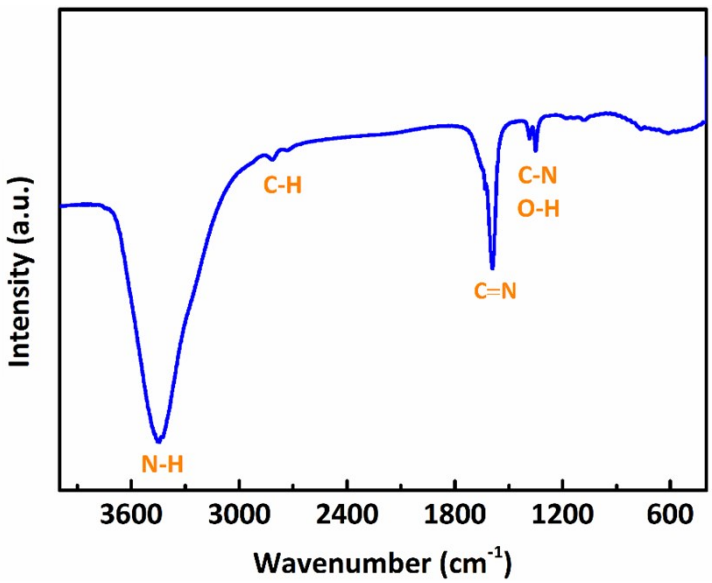

Fig. S6 FT-IR spectra of Co@NPC.

As shown in Fig. S6, the broad absorption band at 3450 cm^{-1} is characteristic of the stretching vibration of N-H bonds. The band at 2820 cm^{-1} is ascribed to the C-H stretching vibration. The band at 1590 cm^{-1} is attributed to the C=N bond stretching vibration, which indicates the presence of N in the porous carbon. Besides, the two bands at 1340-1400 cm^{-1} are related to C-N stretching and the O-H bonds bending vibration.

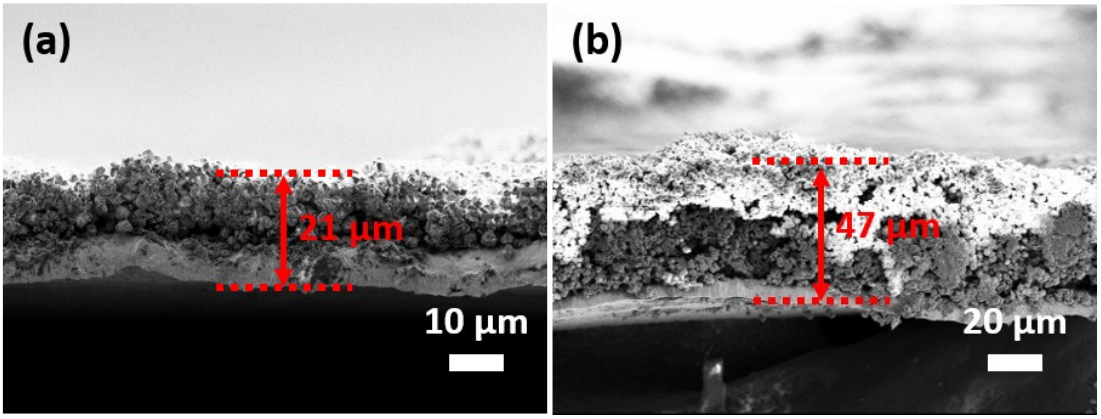

Fig. S7 Cross-section view of (a) ZIF-67/Cu and (b) ICDL/Cu electrodes before cycling.

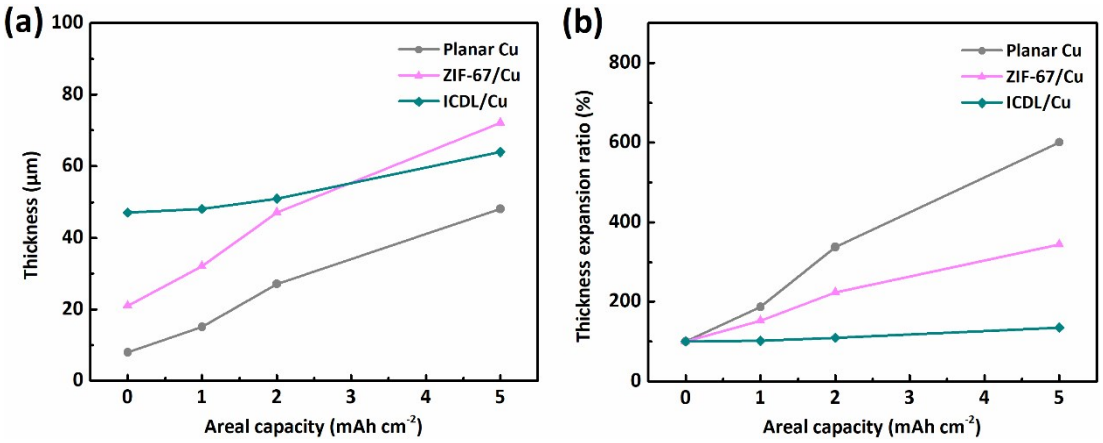

Fig. S8 (a) The thickness changes of planar Cu, ZIF-67/Cu, and ICDL/Cu after plating Li 0 mAh cm^{-2}, 1 mAh cm^{-2}, 2 mAh cm^{-2}, and 5 mAh cm^{-2}, (b) the thickness expansion ratio of planar Cu, ZIF-67/Cu, and ICDL/Cu after plating Li 0 mAh cm^{-2}, 1 mAh cm^{-2}, 2 mAh cm^{-2}, and 5 mAh cm^{-2}.

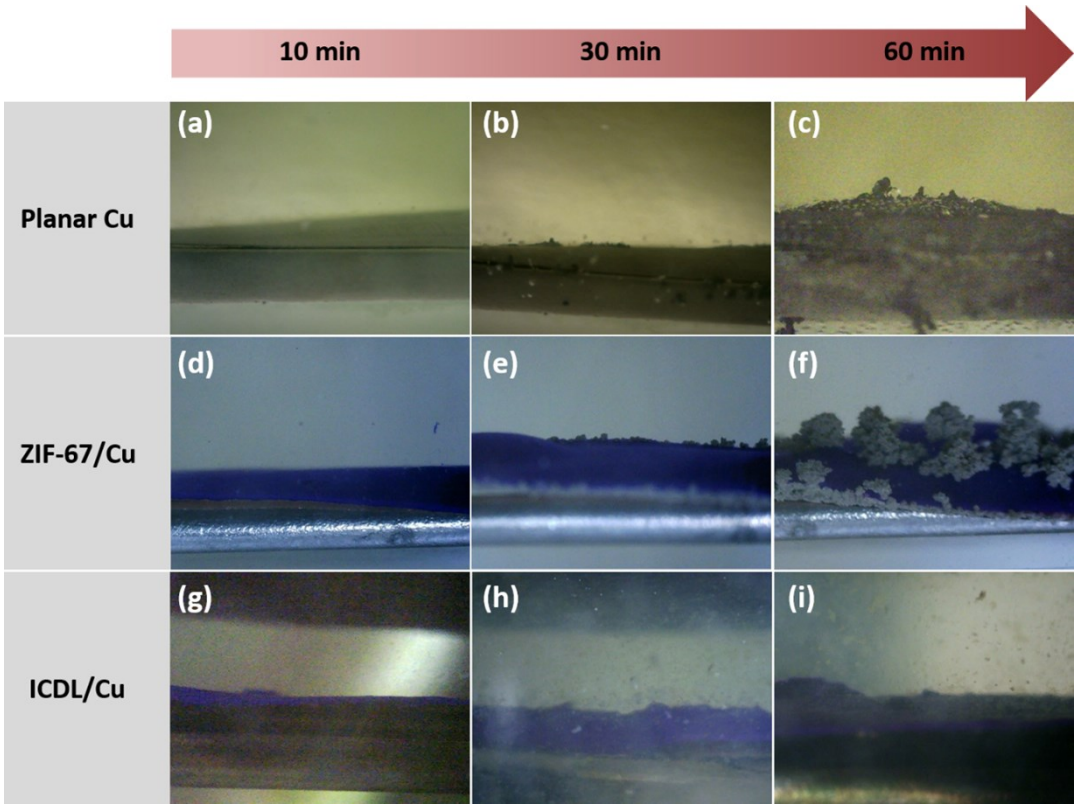

Fig. S9 Optical images of Li deposition on planar Cu, ZIF-67/Cu, and ICDL/Cu-Li for different time at the current density of 3 mA cm^{-2}.

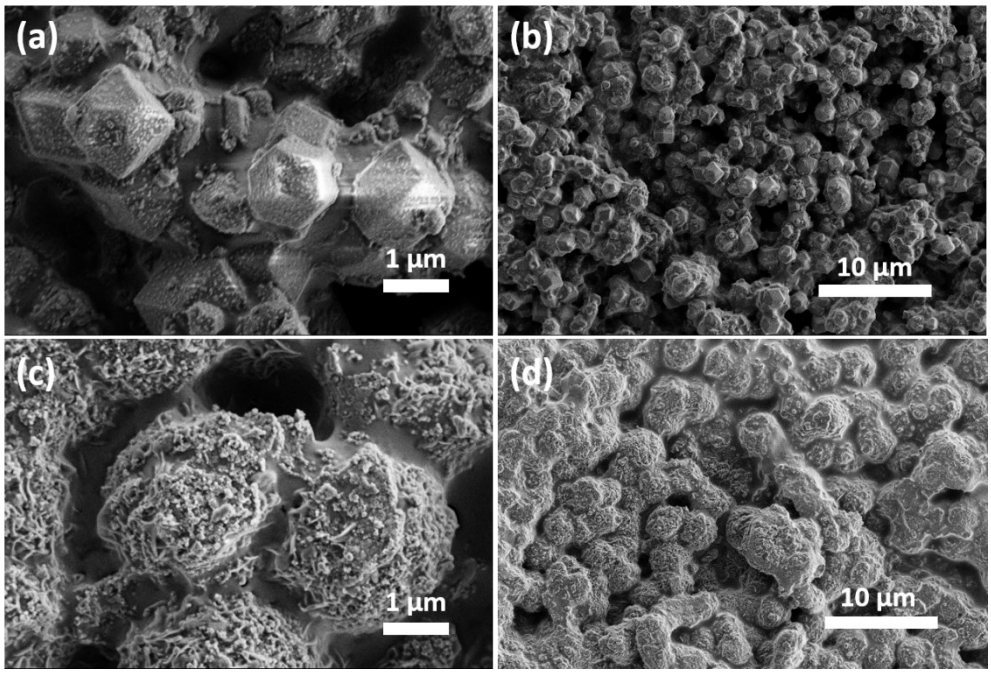

Fig. S10 SEM images of (a) ZIF-67 and (b) carbonized ZIF-67 after Li deposition with a capacity of 1 mAh cm^{-1}.

As shown in Fig. S10a, b, the polyhedral morphology of ZIF-67 is kept well, and the size of ZIF-67 nanoparticles does not change after plating Li, which proves the ZIF-67 coating layer is not involved in Li deposition. After Li deposition, the morphology of Co@NPC nanoparticles is changed significantly, and the Co@NPC is dispersive (Fig. S10c, d), suggesting that Li is firstly deposited on the Co@NPC in the initial Li plating stage due to the strong Li affinity of Co metal nanoparticles and N doped porous carbon.

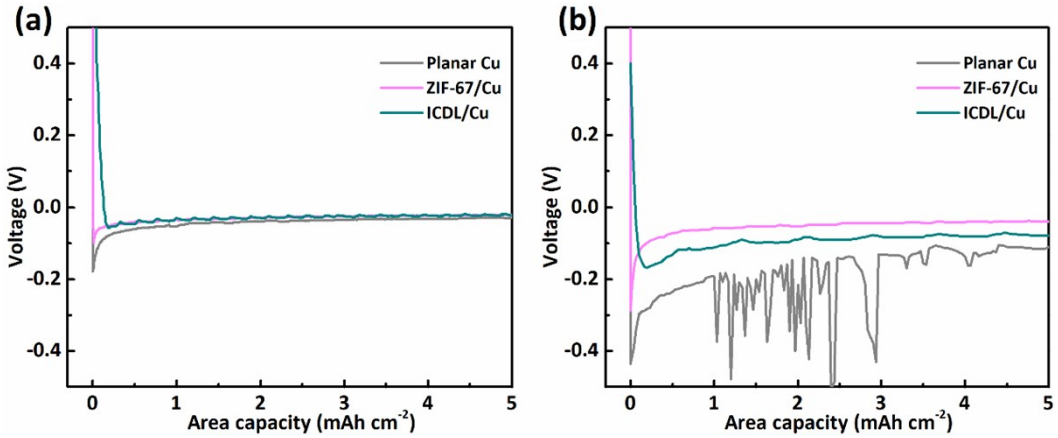

Fig. S11 Comparison of Li nucleation overpotential on the planar Cu, ZIF-67/Cu, and ICDL/Cu at the current density of (a) 0.5 mA cm^{-2} and (b) 3 mA cm^{-2}.

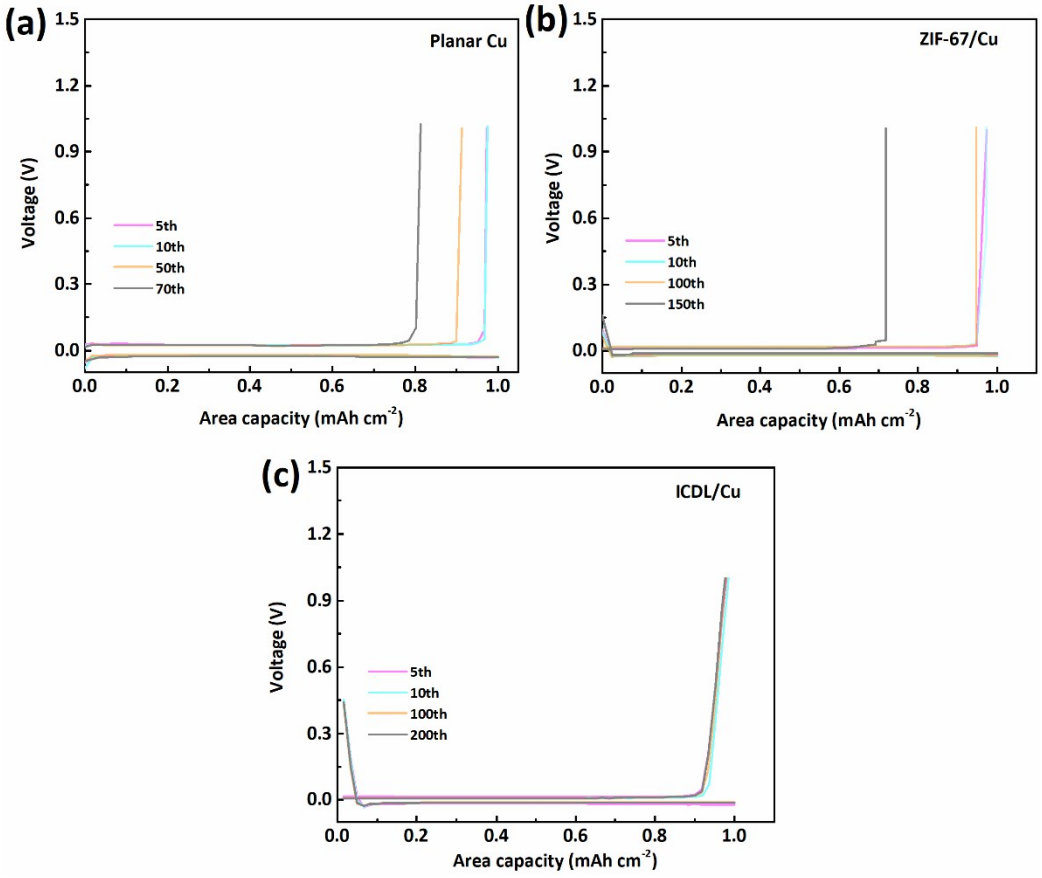

Fig. S12 Voltage profiles of Li plating/stripping of the (a) planar Cu, (b) ZIF-67/Cu, and (c) ICDL/Cu at the current density of 1 mA cm^{-2} for 1 mAh cm^{-2}.

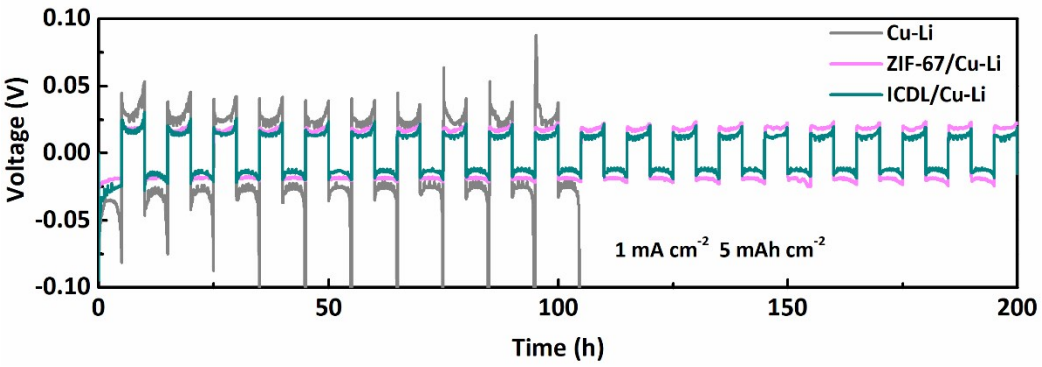

Fig. S13 Comparison of voltage profiles of symmetrical cells at the current density of 1 mA cm^{-1} with the plating/stripping capacity of 5 mAh cm^{-1}.

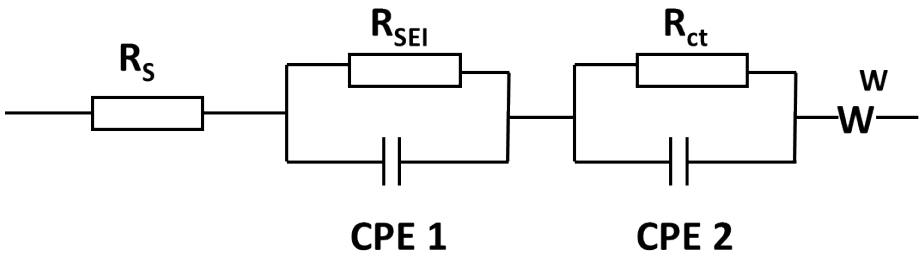

Fig. S14 The equivalent circuit of cells.

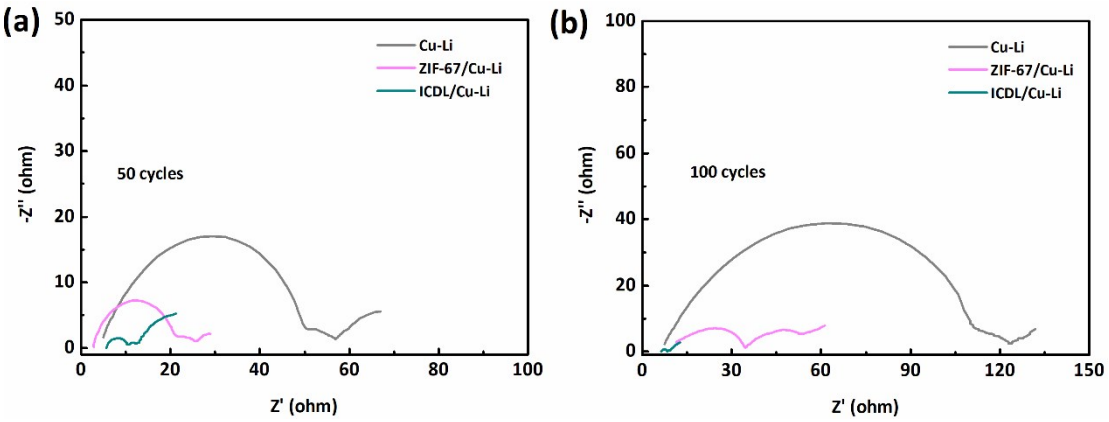

Fig. 15 Nyquist plots of impedance of symmetrical cells after (a) 50 cycles and (b)100 cycles.

After 50 and 100 cycles, the ICDL/Cu-Li||ICDL/Cu-Li symmetrical cell exhibits the smallest values of R_{SEI} and R_{ct} than that of ZIF-67/Cu-Li||ZIF-67/Cu-Li and Cu-Li||Cu-Li. The impedances of ZIF-67/Cu-Li||ZIF-67/Cu-Li and Cu-Li||Cu-Li are gradually increased from 50 cycles to 100 cycles.

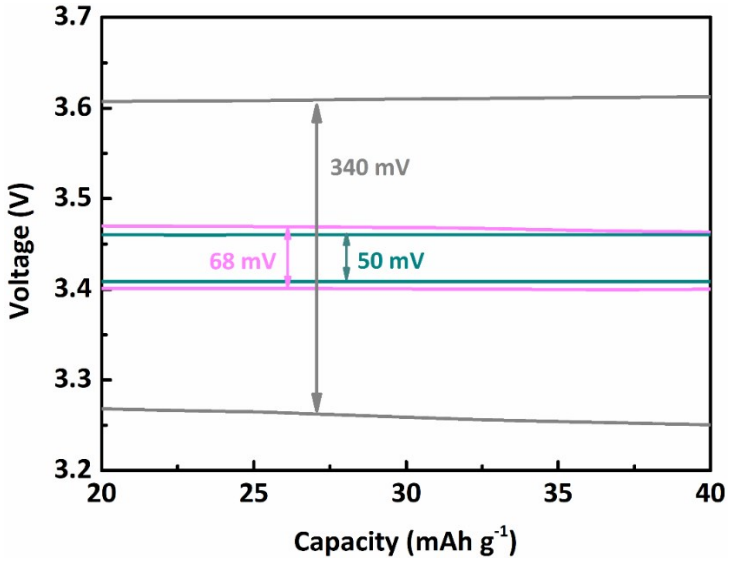

Fig. S16 Voltage polarization of full cells at 1 C.

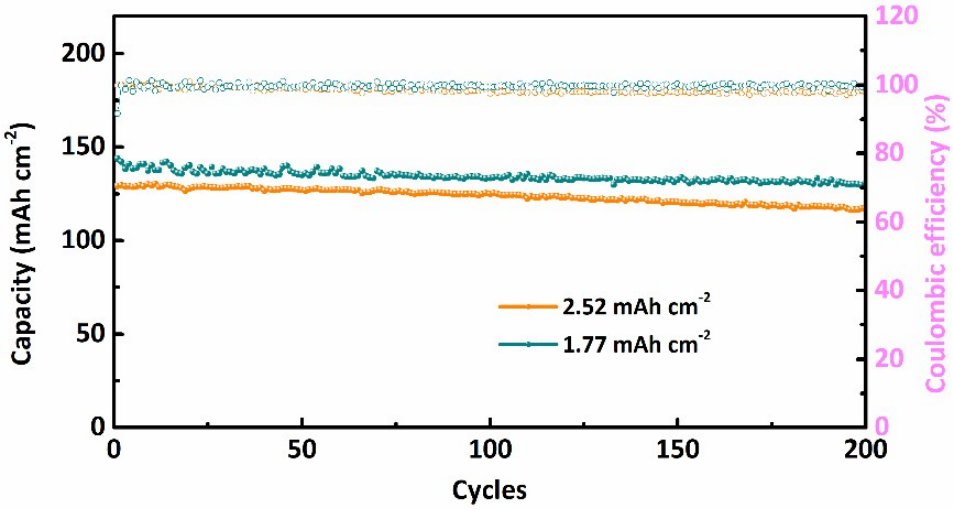

Fig. S17 Comparison of ICDL-Li||LFP cells with different LFP loading.

Table S1 Comparison of symmetrical cell cycling performance between this work and reported literature with the similar electrode configuration.

Composite Li metal anode	Current density-capacity (mA cm^{-2}- mAh cm^{-2})	Hysteresis voltage (mV)	Cycling time (h)	Reference
Li_2CO_3/PVDF	1-1	50	400	1

coated Li				
ZnO-based inorganic/organic double-layer structure	0.5-0.5	~ 100	500	2
LiF/PEO coated Li	1-1	18	1000	3
LiF-rich Li–Sb-Li	1-1	21	500	4
MOF-HCF@Li	1-1	~ 20	1000	5
3D Zn/ZnO-Li	0.5-1	~ 23	900	6
ICDL/Cu-Li	1-1	11	1100	This work

Table S2 The simulated parameters of impedance.

Samples	Cu-Li			ZIF-67/Cu-Li			ICDL/Cu-Li		
Impedance (Ω)	R_s	R_{SEI}	R_{ct}	R_s	R_{SEI}	R_{ct}	R_s	R_{SEI}	R_{ct}
Before cycling	6.2	66.4	15.9	8.3	24.7	23.5	9.6	10.6	14.3
10 cycles	5.3	36.8	10.8	9.4	12.2	11.5	6.9	7.2	6.3
50 cycles	5.2	45.5	7.4	3.7	21.3	4.5	5.8	3.5	2.5

100 cycles	7.7	103.6	17.2	11.1	23.5	20.8	7.2	6.8	5.6

References

1 Y. Liu, S. Liu, S. Tan, Z. Jiang, X. Hu, H. Lu, G. Yin, Y. Gao and Y. Ma, *J. Alloy. Compd.*, 2020, 818, 152862.

2 Y. He, Y. Zhang, X. Li, Z. Lv, X. Wang, Z. Liu and X. Huang, *Energy Storage Materials*, 2018, 14, 392-401.

3 C. Fu and C. Battaglia, *ACS Appl. Mater. Inter.*, 2020, 12, 41620-41626.

4 Y. Zhang, G. Wang, L. Tang, J. Wu, B. Guo, M. Zhu, C. Wu, S.X. Dou and M. Wu, *J. Mater. Chem. A*, 2019, 7, 25369-25376.

5 Z. Zheng, Q. Su, Q. Zhang, X. Hu, Y. Yin, R. Wen, H. Ye, Z. Wang and Y. Guo, *Nano Energy*, 2019, 64, 103910.

6 Q. Chen, Y. Yang, H. Zheng, Q. Xie, X. Yan, Y. Ma, L. Wang and D. Peng, *J. Mater. Chem. A*, 2019, 7, 11683-11689.